Electronic Supplementary Material (ESI) for Physical Chemistry Chemical Physics.
This journal is © the Owner Societies 2024

Electronic Supplementary Information (ESI)

Electronic Structures of Three Anchors of Triphenylamine on a *p*-Type Nickel Oxide (100) Surface: Density Functional Theory with Periodic Models

Outi V. Kontkanen,*[a] Terttu I. Hukka,*[a] and T. T. Rantala [b]

[a] Chemistry and Advanced Materials, Materials Science and Environmental Engineering, Faculty of Engineering and Natural Sciences, P.O. Box 541, FI-33014 Tampere University, Finland.

[b] Physics, P.O. Box 692, FI-33014 Tampere University, Finland.

E-mail: terttu.hukka@tuni.fi

Table of Contents

Computational Details

We use the CRYSTAL09 [1,2] that employs periodic boundary conditions in calculations to relax the geometries, including supercell lattice constant. We apply B3LYP [3,4] hybrid functional and 86411/6411/41 and 8411/411 [5] for surface Ni and O, respectively, and a 6-31G(d,p) [6] for TRIA-ANCHOR basis sets. We use a shrinking factor (SHRINK) of 1 to generate a Monkhorts–Pack type set of a grid of k-points in reciprocal space. We apply tightened tolerance factors of 7, 7, 7, 7, and 14 for Coulomb and exchange integrals (TOLINTEG). We define the atomic spins for Ni according to the AF_2 order, which is described below (ATOMSPIN) and lock the spin states for 20 cycles (SPINLOCK) and add EIGSHIFT to lower the preferred Ni α or β d-orbitals to make the antiferromagnetic AF2 initial guess occupation for the first SCF cycle. In the beginning of the calculations, we allow the SCF change only little (FMIXING 95) during the cycles. However, we decrease the mixing on 25–35 cycles (BROYDEN) from 95 to 70. In addition, SMEAR (0.010) was used to affect the occupation of the orbitals in Fermi level by adjusting the finite temperature.

Calculations of the NiO(100) Surface Slab

In order to model a NiO(100) surface that is a) light enough to calculate, but b) properly describes the surface properties, we performed calculations with various surfaces and keywords. The results are presented in Table S1.

Table S1 *Dependence of the calculated electronic properties of NiO(100) (band gap, E_g, valence band maximum (VBM), and conduction band minimum (CBM)) on the size of the slab model in this work.*

Thickness (layers)	Super-cell	E_g (eV) [a]	VBM (eV)	CBM (eV)
4	2×2	3.96	-4.90	-0.94
8	"	4.43	-5.38	-0.96
2	"	4.50	-5.37	-0.87
2	4×4	3.88	-4.82	-0.95
4	"	3.96	-4.96	-1.00
6 [b]	"	3.92	-4.74	-0.82

[a] Experimental optical band gap of a NiO film: 3.68 eV. [7]

[b] Not fully relaxed.

Our calculations demonstrate that for the 4×4 surface the energy levels are converged for the chosen thicknesses of the model. Thus, it is justified to use a computationally less demanding two layers thick (4×4) slab model to predict the relative tendencies in energies. A large enough area, i.e., 4×4, is important to properly fit the TRIA–anchor molecules onto the model surface. This model also predicts the experimental band gap to a close agreement.

Antiferromagnetic AF2 Phase of NiO

Our model for the NiO(100) surface is antiferromagnetic, i.e., spin states are along the (111) planes, which is demonstrated in Figure S1 with a smaller, four (4) layers thick (2 × 2) supercell model.

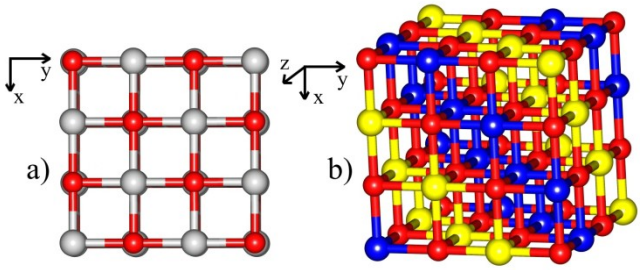

Fig. S1 *Antiferromagnetic phases of NiO. Red presents oxygens atoms (O), yellow nickel (Ni) atoms with spin up, and blue Ni atoms with spins down.*

Binding Energies in Literature

In order to compare the energies of our calculations, we collected adsorption energies ($E_{binding}$) of various anchoring groups presented in literature and grafted onto both the NiO(100) (Table S2) and TiO_2 surfaces (Table S3, respectively). Of these surfaces, TiO_2 is more widely studied.

Table S2 *Various anchoring groups (Anchor) on the NiO(100) surface with the dye basis of the anchor (Dye), grafting type, adsorption energy (E_{bind}, in eV), computational method used (Comp. Meth.), and the reference (Ref.).*

Anchor	Dye	Grating type	E_{bind} (eV)	Comp. Meth.	Ref.
CARB	H-	bidentate	2.68	CRYSTAL PSEUDO, PBE0	[8]
"	Ph-	"	3.84	"	"
"	C343	monodentate	0.59	VASP, PBE+U (U_{3dNi} = 3.8)	[9]
"	"	bidentate	0.71	"	"
$P(OH)_2$ (phosphonic)	CH3	monodentate	0.77	Espresso, PBE+U+d2	[10]
"	"	bidentate	1.36	"	"
"	"	tridentate	0.90	"	"
"	C343	bidentate	1.30	"	"
"	"	tridentate	0.69	"	"
$Si(OH)_3$	Ph	bidentate	8.69	CRYSTAL PSEUDO, PBE0	[8]
$Si((OH)_2)_2$-O	C343	monodentate	0.84	VASP, PBE+U (U_{3dNi} = 3.8)	[9]
"	"	bidentate	1.00	"	"
"	"	tridentate	0.89	"	"

Table S3 *Various anchoring groups (Anchor) on the TiO_2 surface with the dye basis of the anchor (Dye), adsorption energy (E_{bind}), computational method (Comp. Meth.) used, and the reference (Ref.).*

Anchor	**Dye**	E_{bind} **(eV)**	**Comp. Meth.**	**Ref.**
CN(C)COOH	Arylamine	0.87–1.39	Siesta, PSEUDO, GGA	[11]
C_6H_5COOH	-	-1.1–(-0.8)	CRYSTAL06 /Siesta/QE, GGA	[12]
CARB	Perylene	1.26	CRYSTAL98/03, B3LYP	[13]
$P(OH)_2$ (phosphonic)	"	2.21	"	"
CARB	Formic Acid	0.20–1.73	Car-Parrinello, GGA	[14]
CARB	-	2.30–3.62	DFT, HSE06	[15]

The literature review (Table S3 and S4) demonstrates that the fluctuations in adsorption energies (0.59–8.69) eV for NiO and (0.20–3.62) eV for TiO_2 depend on the anchoring group, the dye, grafting and the computational method used in calculations. Concluding from the literature results above, one can assume that if the computational energies fit within the fluctuation range, adsorption is possible on the NiO(100) surface. In addition, the bidentate mode is 0.15–0.65 eV more stable than the monodentate mode, which is to be kept in mind when choosing the accurate theoretical methodology (the B3LYP and PBE functionals with sizable basis set quality). [10] This is also invariant whether the solvent effects are considered with PCM or not.

Energy Levels of the Computed Models

The energy levels calculated in this work[16] are presented in Table S4 and Figures S2–S4 for the separate NiO(100) surface, relaxed, hydrogen free (H-free), and twisted TRIA-anchor dye models, together with their combined, interacting structures, where the H-free anchor models have been used.

Table S4 *Energy levels (in eV) of the separated 2 layers thick 8 × 8 NiO(100) surface, relaxed dyes, dyes with H-free anchors (PYR, CARB, DIOL), twisted dyes, and the interacting models, where H-free anchors were used. CBM and VBM refer to the states of the NiO(100) surface, whereas HOMO and LUMO refer to the energy states of the TRIA-anchor models.*

Separated Models	**CBM (eV)**	**VBM (eV)**	**Relaxed Dye LUMO / HOMO (eV)**	**H-free Anchor LUMO / HOMO (eV)**	**Twisted Dye LUMO / HOMO (eV)**
NiO(100)	-0.96	-4.81	-	-	-
TRIA-PYR	-	-	-1.51 / -5.33	-	-1.57 / -5.44
TRIA-CARB	-	-	-1.65 / -5.62	-2.61 / -6.64	-2.99 / -7.33
TRIA-DIOL	-	-	-0.52 / -4.50	-2.59 / -6.83	-2.32 / -6.57
Interacting Models	**NiO(100) CBM (eV)**	**NiO(100) VBM (eV)**	**Dye LUMO (eV)**	**Dye HOMO (eV)**	**-**
TRIA-PYR	-0.97	-4.83	-1.91	-5.69	-
TRIA-CARB	-0.86	-4.76	-0.74	-4.49	-
TRIA-DIOL	-0.96	-4.81	-2.32	-6.53	-

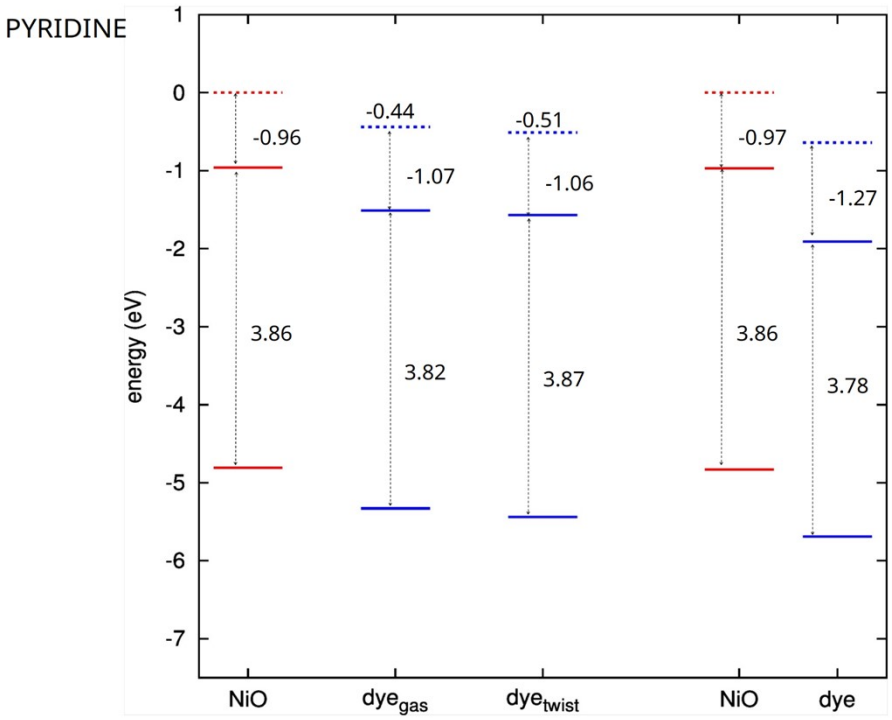

Fig. S2 *Energy levels of the separated NiO(100) surface and the TRIA-PYR-anchors (on the left), and of the interacting TRIA-PYR-anchors and NiO (on the right).*

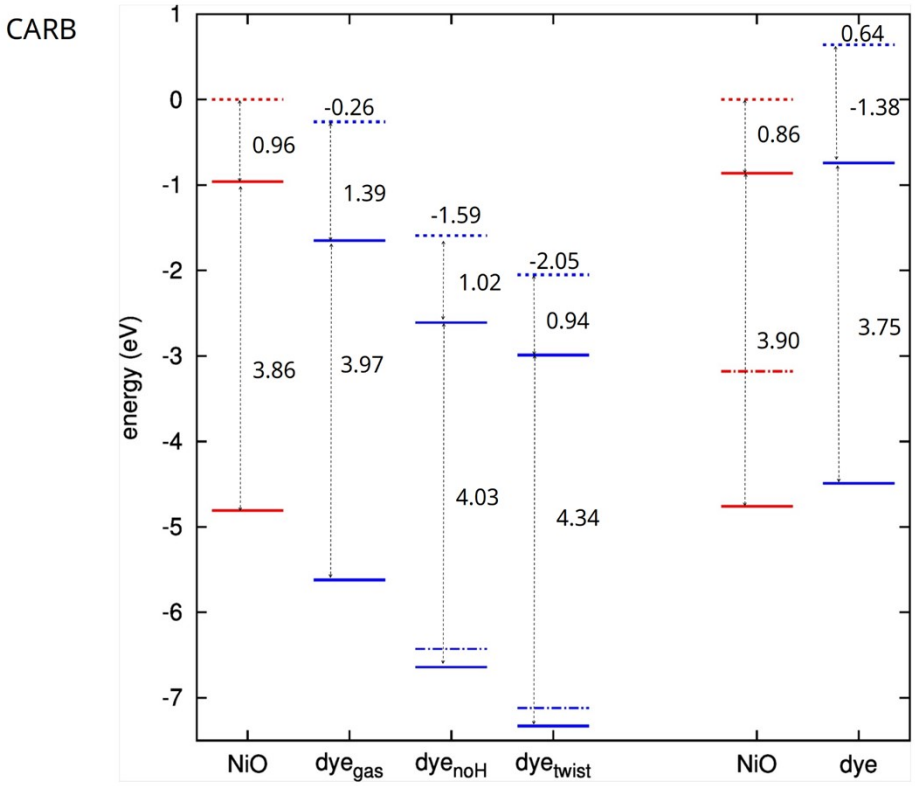

Fig. S3 *Energy levels of the separated NiO(100) surface and the TRIA-CARB-anchors (on the left) and of the interacting TRIA-CARB-anchors and NiO (on the right).*

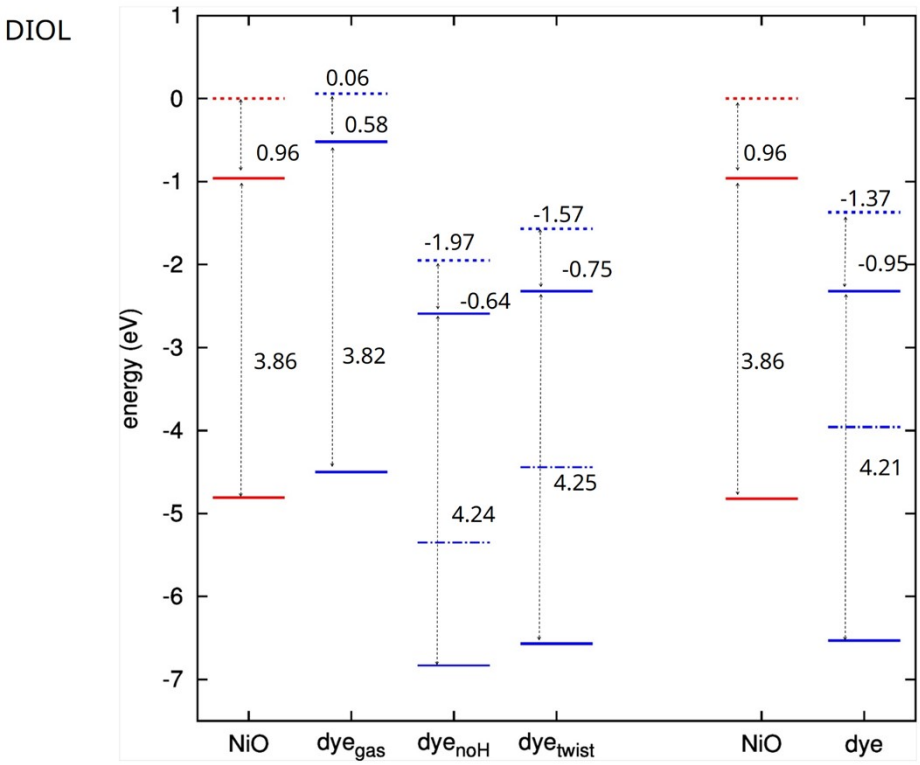

Fig. S4 *Energy levels of the separated NiO(100) surface and the TRIA–DIOL-anchors (on the left) and of the interacting TRIA–DIOL-anchors and NiO (on the right).*

Mulliken Population Analysis

Charges calculated by Mulliken population analysis for the NiO(100), PYR, CARB, and DIOL anchors, and TRIA models are presented in Table S5.

Table S5 *Charges (electrons, el.) from Mulliken population analysis. Negative values refer to given and positive numbers to received electrons by the moiety.*

Anchor on surface	**NiO(100) (el.)**	**Anchor (el.)**	**Triphenylamine Dye (el.)**
PYR	-0.14	0.18	-0.04
CARB	-1.35	0.52	0.83
DIOL	-0.20	0.96	-0.75
Anchor not on surface			
PYR	-	0.07	-0.07
CARB	-	0.28	-0.28
DIOL	-	0.01	-0.01

Molecular Orbitals of the Three Dye–Anchor Models

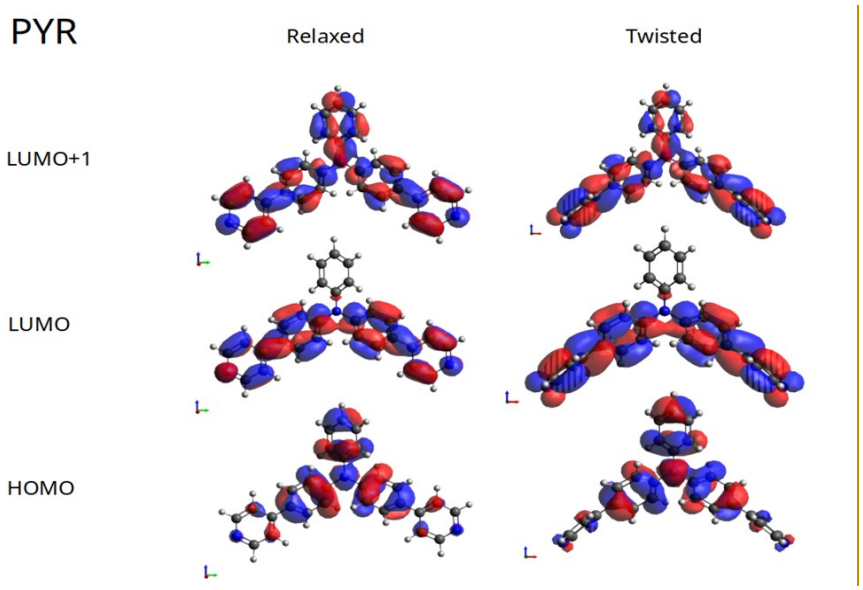

Fig. S5 *Molecular orbitals of the separated TRIA–PYR-anchor models.*

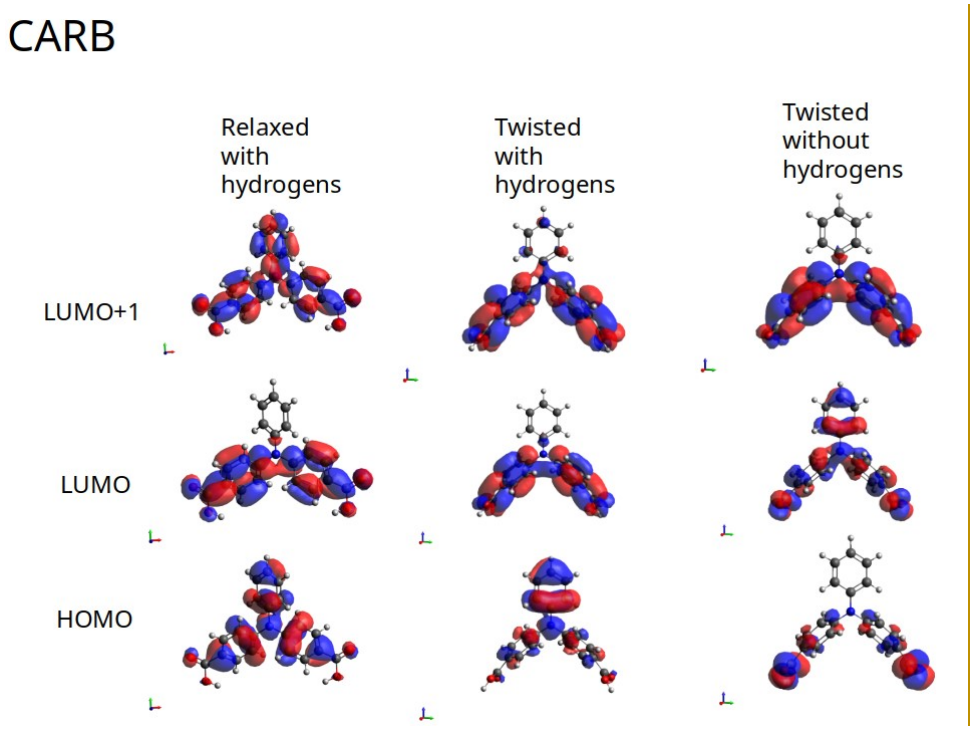

Fig. S6 *Molecular orbitals of the separated TRIA–CARB-anchor models.*

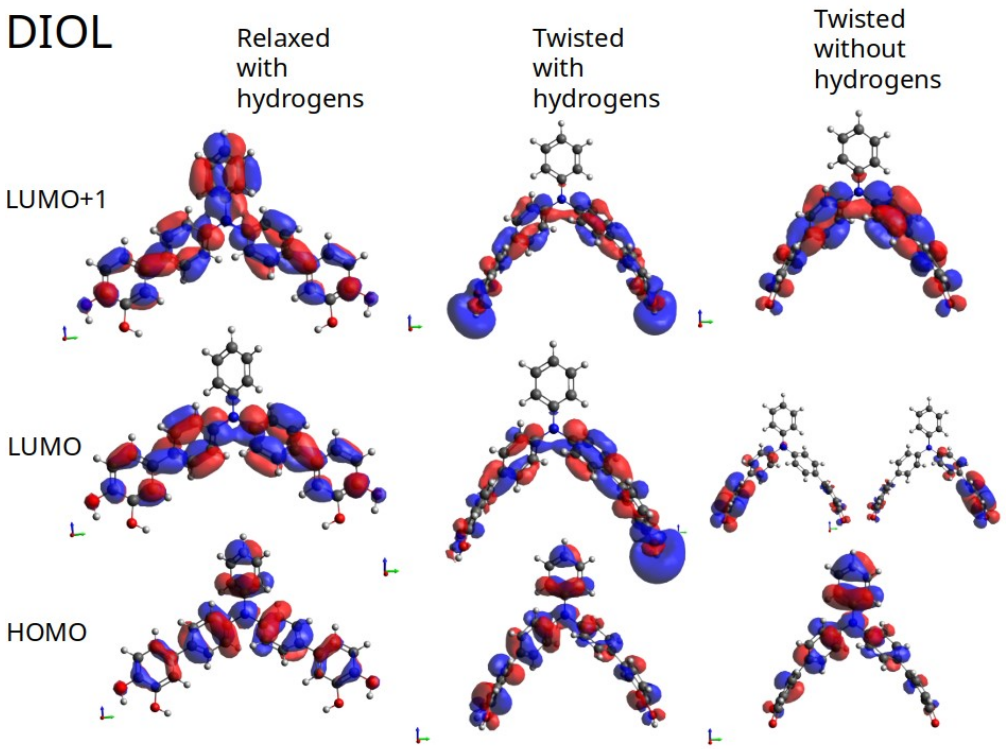

Fig. S7 *Molecular orbitals of the separated TRIA–DIOL-anchor models.*

References

1 R. Dovesi, R. Orlando, B. Civalleri, C. Roetti, V. R. Saunders and C. M. Zicovich-Wilson, CRYSTAL: a computational tool for the ab initio study of the electronic properties of crystals, *Zeitschrift für Krist. - Cryst. Mater.*, 2005, **220**, 571–573.

2 R. Dovesi, V. R. Saunders, R. Carla, O. Roberto, C. M. Zicovich-Wilson, F. Pascale, B. Civalleri, K. Doll, N. M. Harrison, I. J. Bush, P. D'Arco and M. Llunell, *CRYSTAL09 User's Manual*, University of Torino, Torino, 2009.

3 A. D. Becke, Density-functional thermochemistry. III. The role of exact exchange, *J. Chem. Phys.*, 1993, **98**, 5648–5652.

4 W. Kohn, A. D. Becke and R. G. Parr, Density Functional Theory of Electronic Structure, *J. Phys. Chem.,* 1996, **100**, 12974–12980.

5 M. D. Towler, N. L. Allan, N. M. Harrison, V. R. Saunders, W. C. Mackrodt and E. Aprà, *Ab initio* study of MnO and NiO, *Phys. Rev. B*, 1994, **50**, 5041–5054.

6 C. Gatti, V. R. Saunders, Crystal field effects on the topological properties of the electron density in molecular crystals: The case of urea, *J. Chem. Phys.*, 1994, **101**, 10686–10696.

7 Z. Zhang, Y. Zhao, and M. Zhu, NiO films consisting of vertically aligned cone

shaped NiO rods, *Appl. Phys. Lett.* 2006, **88**, 033101. https://doi.org/10.1063/1.2166479.

8 M. Wykes, F. Odobel, C. Adamo, I. Ciofini and F. Labat, Anchoring groups for dyes in *p*-DSSC application: insights from DFT, *J. Mol. Model.*, 2016, **22**, 289.

9 A. B. Muñoz-García and M. Pavone, Structure and energy level alignment at the dye–electrode interface in *p*-type DSSCs: new hints on the role of anchoring modes from *ab initio* calculations, *Phys. Chem. Chem. Phys.*, 2015, **17**, 12238–12246.

10 M. Pastore and F. De Angelis, Modeling Materials and Processes in Dye-Sensitized Solar Cells: Understanding the Mechanism, Improving the EfficiencySpringer, Berlin, Heidelberg, 2013, pp. 151–236.

11 J. Feng, Y. Jiao, W. Ma, M. K. Nazeeruddin, M. Grätzel and S. Meng, First Principles Design of Dye Molecules with Ullazine Donor for Dye Sensitized Solar Cells, *J. Phys. Chem. C*, 2013, **117**, 3772–3778.

12 N. Martsinovich and A. Troisi, High-Throughput Computational Screening of Chromophores for Dye-Sensitized Solar Cells, *J. Phys. Chem. C*, 2011, **115**, 11781–11792.

13 M. Nilsing, P. Persson, S. Lunell and L. Ojamäe, Dye-Sensitization of the TiO_2 Rutile (110) Surface by Perylene Dyes: Quantum-Chemical Periodic B3LYP Computations, *J. Phys. Chem. C,* 2007, **111**, 12116–12123.

14 A. Vittadini, A. Selloni, F. P. Rotzinger and M. Grätzel, Formic Acid Adsorption on Dry and Hydrated TiO_2 Anatase (101) Surfaces by DFT Calculations, *J. Phys. Chem. B,* 2000, **104**, 1300–1306.

15 L. Kou, T. Frauenheim, A. L. Rosa and E. N. Lima, Hybrid Density Functional Calculations of Formic Acid on Anatase TiO_{2} (101) Surfaces, *J. Phys. Chem. C*, 2017, **121**, 17417–17420.

16 O. V. Kontkanen, Modeling of Charge Transfer at Dye-Semiconductor Interfaces in p-Type Solar Cells. Tampere University of Technology, 2018. https://urn.fi/URN:ISBN:978-952-15-4107-0.